nature materials

PERSPECTIVE

https://doi.org/10.1038/s41563-018-0075-8

Materials challenges for the Starshot lightsail

Harry A. Atwater[1*], Artur R. Davoyan[1], Ognjen Ilic[1], Deep Jariwala[1], Michelle C. Sherrott[1], Cora M. Went[2], William S. Whitney[2] and Joeson Wong[1]

The Starshot Breakthrough Initiative established in 2016 sets an audacious goal of sending a spacecraft beyond our Solar System to a neighbouring star within the next half-century. Its vision for an ultralight spacecraft that can be accelerated by laser radiation pressure from an Earth-based source to ~20% of the speed of light demands the use of materials with extreme properties. Here we examine stringent criteria for the lightsail design and discuss fundamental materials challenges. We predict that major research advances in photonic design and materials science will enable us to define the pathways needed to realize laser-driven lightsails.

The Starshot Breakthrough Initiative has challenged a broad and interdisciplinary community of scientists and engineers to design an ultralight spacecraft or 'nanocraft' that can reach Proxima Centauri b — an exoplanet within the habitable zone of Proxima Centauri and 4.2 light years away from Earth — in approximately 20 years[1,2]. Such a spacecraft, represented pictorially in Fig. 1, would consist of two components: a lightsail propelled by laser radiation pressure, and a payload or 'StarChip' that contains the electronics and sensors necessary to gather data and transmit it back to Earth[1]. The proposed concept is inspired by the existing body of work on solar sails[3,4], most notably the IKAROS (Interplanetary Kite-craft Accelerated by Radiation of the Sun) mission launched in 2010[5]. The IKAROS spacecraft uses sunlight as the source of radiation pressure, its sail consisting of a thin (7.5 μm) polyimide film with a subwavelength (80 nm) aluminium reflective coating that provides ~80% specular reflectivity. Equipped with thin-film solar cells and reflectivity-control devices (RCD) for attitude control, it can reach a maximum velocity of 400 m s^{-1} (ref. [6]). By contrast, the Starshot Breakthrough Initiative aims to launch a nanocraft that reaches a relativistic speed of ~60 000 km s^{-1} (20% the speed of light) using radiation pressure from a high-powered phased array of lasers on Earth (~10 GW m^{-2} of net laser intensity). Though the methodology of the IKAROS project can provide useful guidelines for light-based propulsion of miniature spacecrafts, the targets of the Starshot mission — in particular, the need to achieve a velocity five orders of magnitude greater — demand a strikingly different approach. The Starshot effort envisions propulsion using a laser system capable of continuous wave power generation at the 50–70 GW level for an impulse of approximately 1,000-second duration[2,7]. This laser system is likely to be an optically dense phased array of individual laser elements such as kW-scale solid-state diode laser amplifiers that are phase locked when fed by a common seed laser[8–10].

In order to reach relativistic speeds, the Starshot lightsail should have an area of ~10 m^2 and be kept to a mass of under ~1 gram, which translates into an equivalent thickness of approximately 100 atomic layers. The design of the lightsail will therefore need to push the boundaries of materials science, photonic design and structural engineering to enable high performance with minimal mass.

In this Perspective, we identify key design criteria and fundamental material challenges for the Starshot lightsail. Specifically, we discuss materials with extreme optical, mechanical and thermal properties required for the design of the lightsail. For such a laser-driven nanocraft, we reveal a balance between the high reflectivity of the sail, required for efficient photon momentum transfer; large bandwidth, accounting for the Doppler shift; and the low mass necessary for the spacecraft to accelerate to near-relativistic speeds. We show that nanophotonic structures may be well-suited to meeting such requirements. Such structures may include two-dimensional photonic crystal slabs[11], where periodic nanostructures in a thin dielectric slab open up a photonic bandgap; metasurfaces, where arrays of resonant elements can be collectively excited to modify their reflection profile[12]; or 1D photonic crystals, where alternating layers of high and low refractive index can result in a spectral band of high reflectivity[11]. In each design, the combination of material properties and nanostructure will be crucial for minimizing mass while maximizing photon momentum transfer.

With radiative cooling being the sole mechanism for passive thermal management in space, we quantify stringent requirements on material absorptivity that enable the lightsail to withstand high laser intensity and prevent excessive heating and mechanical failure. Materials selected to form the lightsail must have extremely low optical losses (absorptivity $<10^{-5}$) in the near-infrared (IR) at elevated temperatures, placing strong constraints on the design space and requiring the consideration of fundamental limits to absorption imposed by different absorption mechanisms in materials. To better understand and characterize the limiting absorption mechanisms, we propose a renewed effort for ultrasensitive measurements of the optical properties of candidate materials, including the use of techniques such as photothermal deflection spectroscopy and photoacoustic spectroscopy. In addition, the extreme constraints on the mass of the nanocraft necessitates the use of materials in ultrathin-film form. Consequently, we discuss several approaches for synthesis, fabrication, assembly and handling of materials in such ultrathin, but macroscopic, structures.

Lastly, we discuss the requirements for nanocraft stability during acceleration phase. We show that together with photonic and thermal considerations, important factors such as the sail shape, beam profile and mechanical properties must be considered. Importantly, we argue that a successful design of the lightsail will require synergetic engineering: simultaneous optimization and consideration of all of the parameters described above.

In this Perspective, we address the above issues and offer a positive outlook on the challenges and opportunities for designing the Starshot lightsail based on these constraints, and suggest pathways

[1]Department of Applied Physics and Materials Science, California Institute of Technology, Pasadena, California, USA. [2]Department of Physics, California Institute of Technology, Pasadena, California, USA. *e-mail: haa@caltech.edu

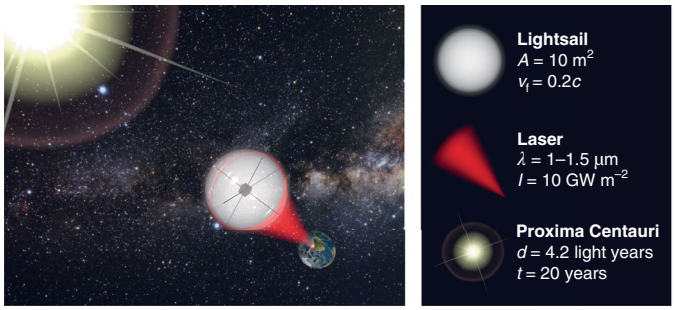

Fig. 1 | Vision for the Starshot nanocraft. A phased array of lasers, or a light beamer, will propel the nanocraft towards Proxima Centauri. The nanocraft consists of the lightsail, discussed in this Perspective, and a nanochip that will collect data to transmit back to Earth.

for realizing the ambitious goal of sending a spacecraft to Proxima Centauri b, our closest known exoplanet.

Choice of materials

The first critical step towards practically realizing the spacecraft depicted in Fig. 1, which can travel at relativistic speeds, is materials selection for the sail. Because the mechanism for propulsion is momentum transfer of reflected photons, the sail materials must offer sufficient optical contrast while minimizing absorption. For a ground-based laser array, considerations of the size (and cost) of the system, together with peaks in atmospheric transparency, imply that the near-IR spectral window (1–2 μm) is of particular interest. While several noble metals such as gold and silver are excellent reflectors in the propulsion wavelength range, they still have sufficient absorption from free carriers to prevent survival at 10 GW m^{-2} incident power densities[13]. Therefore, the efficient transfer of laser photon momentum must be achieved by an appropriate photonic design and with the use of high refractive index contrast. Semiconducting materials typically have high refractive indices just below the band edge transition energy that coincide with a decrease in absorption.

In order to evaluate materials based on the above criteria, we focus on semiconductors with sub-band energies in the near-IR. A quantitative comparison of refractive indices among these materials shows that semiconducting chalcogenides of molybdenum and tin have the highest refractive indices ranging from ~4.3 for $MoSe_2$ (ref. [14]) to 4.0 for SnS (ref. [15]), followed by both crystalline and amorphous silicon at ~3.5. Germanium monochalcogenides[15] and GaAs (ref. [16]) also have refractive indices >~3 below their absorption band edge. The high refractive index of such materials, however, comes with a comparatively high mass density, due to heavier constituent atoms. In addition to chalcogenides, other interesting materials are diamond and silicon due to their low mass density and moderately high index of refraction.

In Fig. 2, we compare several candidate materials, based on their refractive index, mass density and the sub-gap absorption coefficient[17–23] (here we use experimental data based on the photothermal deflection or photocurrent spectroscopy, averaged over the 1–1.5 μm wavelength range). While a number of materials have one superlative figure of merit, none of them appear to lie in the ideal region of high refractive index, low absorption coefficient and low mass density. Nonetheless, the materials plotted in Fig. 2 can be further shortlisted if they meet at least two of the three figures of merit. This reduces the list of potential materials to a-Si and c-Si, both of which possess low absorption, low mass density and high index; diamond with moderately high index, low absorption and moderate mass density; and finally MoS_2 with highest index, moderately high absorption and moderate mass density. The level of absorption

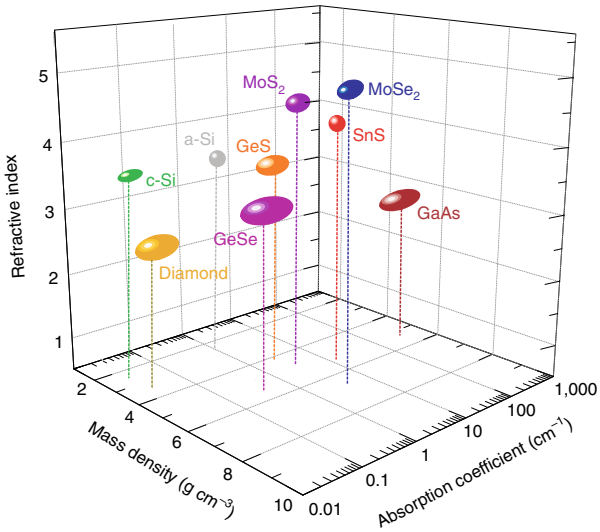

Fig. 2 | Materials candidates for the Starshot lightsail. Refractive index, absorption coefficient (cm^{-1}) and mass density (g cm^{-3}) are shown for several candidate materials, revealing the trade-off between high refractive index (chalcogenides) and low absorption and mass density (silicon and diamond). Absorption coefficient values are averaged in the 1–1.5 μm range and reported from photothermal deflection spectroscopic measurements.

is highly sensitive to the material quality and defect/impurity density as will be discussed in detail later. Therefore, the plotted values of absorption for any given material can be reduced further with higher crystalline quality of the material.

Lightsail photonic design

An effective photonic design of the lightsail should seek to maximize the momentum transfer from the impinging laser light. A key consideration is the notion that, as the sail accelerates to its target final velocity v_f, the photons from the laser (λ_0) are redshifted due to the Doppler effect ($\lambda_f = 1.22\lambda_0$ for $v_f = 0.2c$). This implies that a lightsail should have sufficiently high reflectance in the range of relevant wavelengths [λ_0, λ_f], set by the target velocity v_f. While the ultimate shape of the lightsail will be determined by stability considerations, the constitutive elements of the sail can assume a variety of forms: from single slabs of material to more advanced photonic structures, such as multilayer stacks or photonic-crystal (PhC) slabs. These are shown in Fig. 3, where we explore a range of photonic designs to propel the sail to relativistic speeds. Based on the considerations of material refractive index, absorption and mass density from Fig. 2, we explore crystalline silicon (c-Si) and molybdenum disulfide (MoS_2) as promising material candidates for the lightsail.

Conventional wisdom implies that a lightsail should have a very high reflectance to maximize the momentum transfer per reflected photon. For each type of structure shown in Fig. 3 (slabs, multilayer stacks, photonic crystal pillars and photonic crystal holes), we employ nonlinear optimization to find designs that maximize the average reflectance in the [λ_0, $1.22\lambda_0$] range (in order to reduce absorption, we assume sub-bandgap laser wavelengths, specifically λ_0 = 1.2 μm for c-Si, λ_0 = 1.0 μm for MoS_2). From Fig. 3a,b we see that both the three- and the five-layer stacks, as well as the PhC slabs, can approach near-unity reflectance. For the three- and the five-layer stacks, we assume that intermediate layers have unity refractive index. In practice, this could include low-index, low-weight materials, such as aerogels[24–28].

However, while various photonic structures can be optimized to have high reflectance, optimizing solely for reflectance can result in structures with large per-area mass. A more relevant optimization

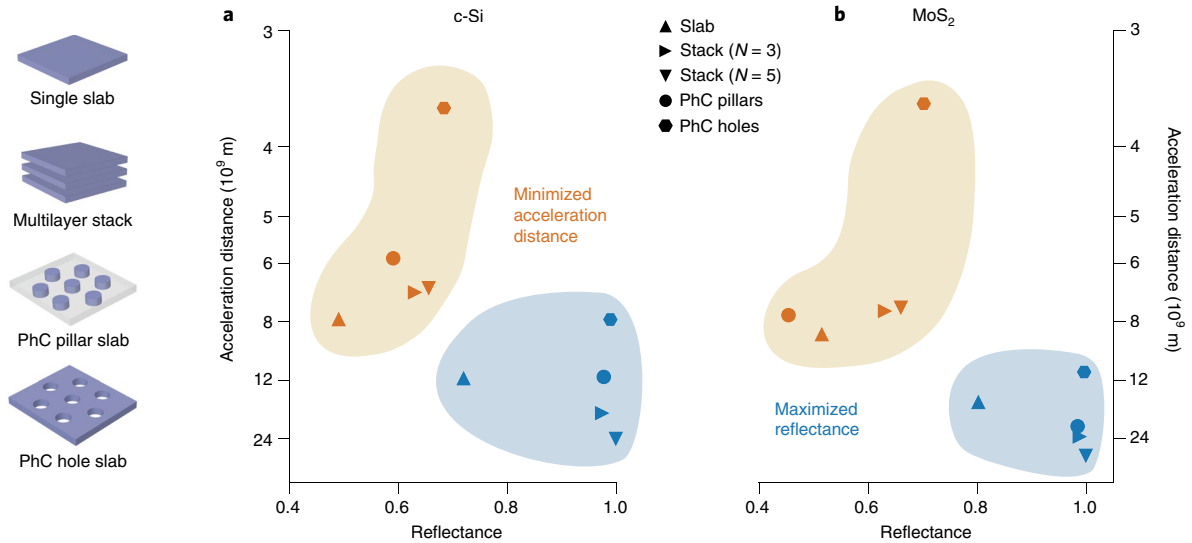

Fig. 3 | Photonic design of the Starshot lightsail. a, A concept of a lightsail consisting of a crystalline silicon (c-Si) slab, multilayer stack, photonic crystal (PhC) slab of pillars, or a PhC slab of holes. For each type of structure, we find the optimal design that maximizes the average reflectance (blue) or minimizes the acceleration distance to v_f (orange). **b**, Same as **a** only for molybdenum disulfide (MoS_2). For both materials, optimal structures (PhC hole slabs, labelled as orange hexagons) reach v_f in ≈150 s. All photonic structure optimizations assume a specific payload mass (0.1 g), laser intensity (10 GW m^{-2}), sail area (10 m^2), and target velocity ($v_f = 0.2c$). The reflectance is averaged over the Doppler-shifted spectral range [λ_0, 1.22λ_0] (where the operating laser wavelength $\lambda_0 = 1.2$ μm for c-Si and $\lambda_0 = 1.0$ μm for MoS_2).

figure of merit (FOM) would also take into account the total mass of the spacecraft (lightsail and the payload). Among several possible FOMs, here we focus on minimizing the acceleration distance (D). The acceleration distance is the total travelled distance to reach the desired velocity (v_f) and can be approximated, for example, by[4,29]

$$D(v_f) \sim \left(\frac{c}{2IA}\right) \int_0^{v_f} \frac{m_T}{R(v)} \frac{\gamma(v)v}{\left(1-\frac{v}{c}\right)^2} \mathrm{d}v \qquad (1)$$

where $m_T = m_{sail} + m_{payload}$ is the total mass of the spacecraft, and $R(v)$ is the (instantaneous) reflectance of the sail for the Doppler-shifted light. Here A is the area of the sail, I the laser intensity, and $\gamma(v) = 1/\sqrt{1-v^2/c^2}$ is the Lorentz factor. Minimizing acceleration distance is relevant from the point of view of the size (and cost) of the Earth-based laser array: the longer the acceleration distance the larger the diffraction-limited laser array[2].

From Fig. 3a,b, we observe that structures that minimize the acceleration distance D (orange) sacrifice high reflectance for a significant decrease in weight. For both crystalline silicon and MoS_2, a properly designed hexagonal lattice of holes achieves the target v_f in ~150 s and in less than half the distance of any of the designs that maximize reflectance (for c-Si, the structure has a period of $a = 1.24$ μm, thickness $t = 59$ nm and hole radius $R = 490$ nm; we assume $m_{payload} = 0.1$ g). For crystalline silicon, such structures also have ultralow absorption: the maximum absorption in the [λ_0, 1.22λ_0] wavelength range is ~2.5×10^{-7}. This could further be reduced by noting that the absorption coefficient of c-Si can become smaller with increasing wavelength in the near-IR; hence, a slight shift in propulsion laser wavelength to, for example, $\lambda_0 = 1.25$ μm would result in a tenfold decrease in maximum absorption.

This short analysis shows that subwavelength structures could achieve the desired optical response over the Doppler-shifted bandwidth while maintaining low mass and points to alternative figures of merit (for example, minimizing the acceleration distance) that may be more relevant. Given the interplay between reflectance, mass and material absorption, we can identify nanophotonic designs with ultralow absorption that are very light yet provide substantial optical contrast. While a real-life lightsail (and the corresponding laser array) is a complex system with multiple competing considerations, these results show that incorporation of nanophotonic elements could benefit the lightsail design. Here we explored the relevant parameter space through (multistart) local, derivative-free optimization[30] (as such, the resulting designs, where total material thicknesses are approximately in the 20–60 (100–400) nm range for acceleration distance (reflectance) optimizations, are not guaranteed global optima). However, we also envision the use of inverse design and topology optimization, methods commonly used in aerospace design and, more recently, in photonics[31–33]. Subsequent challenges would include the integration of many such nanophotonic structures — with multiple functionalities — into the overall lightsail design in order to address the issues of propulsion stability, tensile stress redistribution, and off-normal light incidence. Any lightsail design would naturally have to exhibit sufficient structural integrity and be compatible with the mechanical stresses during the launch and the deployment phases. To that end, the experience of large-area sheet deployment of the IKAROS mission could be leveraged, or potential alternative methods of protective encapsulation be explored (for example, a sacrificial casing that is laser-ablated in the pre-acceleration stage).

Challenges of the launch and the acceleration phase also include the interaction of the lightsail with atoms or particulates in the interplanetary medium. For interactions with atoms, hydrogen and helium represent the predominant form (>90%)[2,34,35] of gas found in outer space. The severity of damage from these light atoms is not yet clear on the nanometre-scale photonic structures proposed for the sail. Indeed, Hoang et al.[36] calculated the average penetration depth of hydrogen and helium to be ~1 mm at 0.2c, suggesting these particles may pass through the lightsail with little interaction. In the case of cosmic dust particles that are generally more massive — mean mass of ~10^{-16} kg (ref. [37]) — the damage could be more severe.

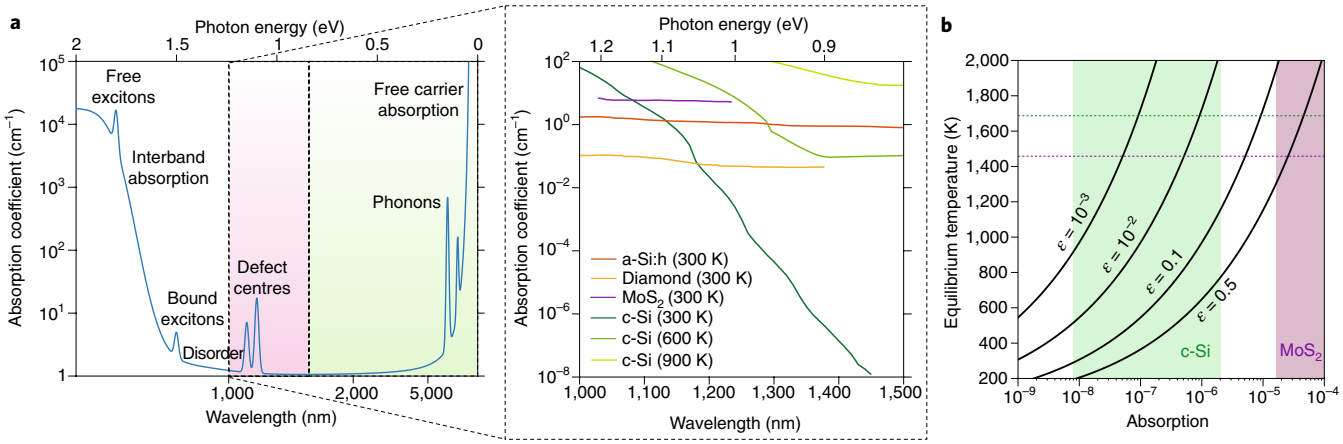

Fig. 4 | Absorption mechanisms and values. a, Schematic description of absorption mechanisms at visible to mid-infrared wavelengths. The region of laser illumination is highlighted in red, in which low absorptivity is necessary. The region of likely thermal emission is highlighted in green, in which high emissivity (and hence absorptivity) is desired. Inset: experimental and modelled absorption coefficient values for low-absorption lightsail candidate materials in the laser illumination wavelength band. **b**, Equilibrium lightsail temperature as a function of its emissivity and absolute absorption. Shaded areas correspond to absolute absorption ranges for the c-Si and MoS_2 lightsail structures simulated in Fig. 3. Dashed lines indicate the corresponding melting temperatures of c-Si and MoS_2.

However, the interplanetary dust density of 10^{-8} m^{-3} (ref. [2]) is much lower than the typical hydrogen gas density of 10^6 m^{-3}, suggesting an interaction with of order 1,000 dust particulates over the acceleration distance of ten billion metres, and 10^9 over the full distance to Proxima Centauri. While the damage induced by these particles will be strongly dependent on both the sail material and shape, the likely damage modes are examined by Hoang and colleagues[36]. For an ultrathin, planar or spherical sail, typical dust particles of diameter 0.3 μm or smaller are likely to melt or vaporize their columnar trajectories through the sail, inducing structural damage and heating. However, for a 10 m^2 sail, 10^9 such micrometre-wide trajectories represent, collectively, less than a tenth of a percent of the total sail area. As a result, we expect that for a judicious choice of sail design, a single sail will be likely to survive the interstellar medium en route to its destination. Furthermore, the survival of the lightsail itself may only be critical during the acceleration phase, during which the fractional area of damage is orders of magnitude lower than estimated above. The potential additional impact of solar winds and flares can be minimized through atmospheric prediction and suitable choice of launching times. We pose, though, that damage tolerance is an important area for future study for both the lightsail and the StarChip payload, the latter of which must survive its entire voyage functional. Lastly, we emphasize that the project envisions launching a large number of such spacecraft, in an effort to increase the likelihood of success of all mission components.

Lightsail thermal management

To enable successful thermal management of the lightsail during illumination, strict constraints exist on material absorptivity and emissivity. Unlike the macroscopically thick IKAROS sail, where front-side reflectivity and back-side emissivity could be independently optimized for efficient momentum transfer and radiative cooling, the ultrathin Starshot lightsail may need to achieve both functionalities in a single component. As previously discussed, ultralow absorptivity is required in the (Doppler-shifted) wavelength range of laser illumination to avoid catastrophic overheating. At the same time, high emissivity is necessary at wavelengths outside that band to allow efficient radiation of thermal energy and maintain equilibrium sail and payload temperatures below critical failure thresholds. By Kirchoff's law of thermal radiation, high emissivity also implies high out-of-band absorptivity. This pair of constraints challenges conventional materials and will provide an opportunity for contributions from engineered materials and photonic structures.

Fundamental material absorption is driven by several physical mechanisms, the most important of which are outlined in Fig. 4a. At short wavelengths above the bandgap, interband optical transitions dominate, superimposed in some systems with excitonic effects near the band edge. In disordered materials, an Urbach tail of substantial sub-gap interband absorption may also exist. Narrow, defect-derived absorption features such as colour centres introduce further absorption, typically at near-infrared or bluer wavelengths. Lastly, at long wavelengths phonon lines and free carrier absorption generate strong absorption and therefore emission.

An ideal lightsail material will lack most of these absorption mechanisms in the targeted (~1–1.5 μm) illumination band, which is achieved in several real materials, including c-Si, a-Si, diamond and MoS_2. Absorption coefficients for these materials in this range are plotted in Fig. 4a, and are typically limited by material quality[18,19,21,38]. With improved growth processes, it may be possible to achieve significantly lower absorption. However, most materials — including the ones considered in this Perspective — lack significant absorption features between the band edge and the onset of phonon absorption lines in the mid- to far-infrared. This window of minimal absorption and emission contains the peak of blackbody emission for likely sail temperatures — of order 500 to 1,500 K — and so presents a challenge for thermal emission.

As the lightsail loses heat radiatively, its equilibrium temperature during illumination will depend strongly on its emissivity. In Fig. 4b, we illustrate the equilibrium temperature achieved for different combinations of sail absorption (in the laser band) and emissivity (outside the laser band). If emissivity falls below 10^{-3}, it is likely that insufficient power will be radiated to avoid material melting or other thermal failure modes. In addition, resonant nanophotonic elements can also increase absolute absorption. To combat this problem, an important challenge will be to use nanoscale structures to enhance thermal radiation emission from the lightsail at relevant wavelengths despite inherently low intrinsic material emissivity — for example, incorporating a thin (~50 nm) layer of SiO_2 could provide the adequate hemispherical emissivity (~1%) due to increased absorption in the IR (>5 μm). An additional challenge for materials researchers will be to use defect engineering to generate tailored materials with elevated inherent emissivity in the mid-infrared, and low absorption in the laser illumination band.

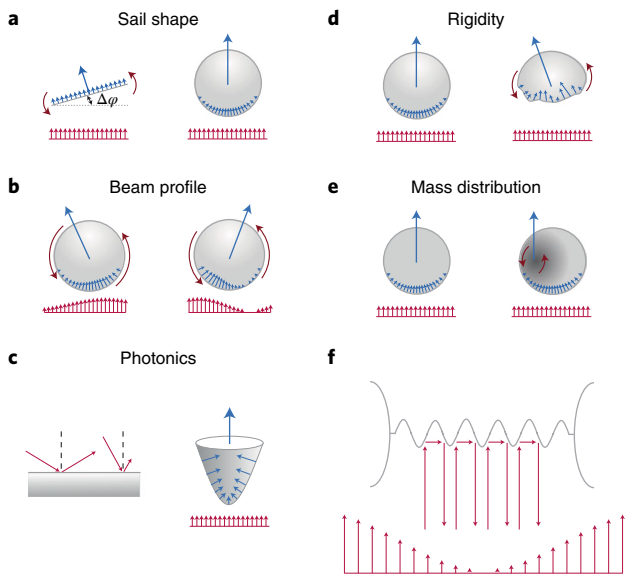

Fig. 5 | Sail design and stability. a–e, Key design considerations for the stability of a laser propelled spacecraft. **f**, A conceptual illustration of a possible sail design, where all of the design parameters are taken into account using modular components. Here red arrows denote schematically laser beam illumination, blue arrows correspond to local and total laser induced forces.

Lastly, the temperature dependence of material absorption properties must be considered to accurately assess absorption in a 500 to 1,500 K sail. For semiconducting materials, previous measurements show that absorption in the laser illumination band increases drastically with temperature, as the thermally generated carrier population grows exponentially[38]. For c-Si, for example, an increase in temperature from 300 K to 900 K results in an increase in absorption coefficient of several orders of magnitude. This trend is illustrated in the inset of Fig. 4a, which includes modelled c-Si absorption data across multiple temperatures[39,40]. The use of wider bandgap materials may be necessary to mitigate such thermally driven increases in absorption[38]. For many materials, though, experimental reports of the temperature dependence of below-gap absorption do not exist. We propose that characterization of these temperature-dependent material properties is an important area for future research.

More broadly, there is an urgent need to better understand the absorptivity and emissivity of candidate materials for the lightsail. Many existing measurements of material absorption focus on the band edge spectral region, or lack the sensitivity to characterize absorption at the ultralow levels required for the lightsail project. For some emerging materials, even the refractive index may be poorly characterized. We propose a renewed effort for ultra-sensitive measurements of the optical properties of these and other materials, by use of techniques such as photothermal deflection spectroscopy (PDS)[41,42], photoacoustic spectroscopy (PAS)[43], and resonant absorption by integrating the candidate materials with high-Q optical cavities[44,45]. For example, both PDS and PAS spectroscopy are non-destructive techniques typically used to measure sub-gap absorption for characterizing impurity, surface and defect states in semiconductors[20,22,46,47]. Values of product αl, where α is the absorption coefficient and l is the thickness of the material, as low as 10^{-8} have been measured for liquid samples[41]. Thus, for materials available in bulk sizes (~1 cm in one dimension at least) most configurations of PDS and PAS will be able to measure sub-gap absorption down to 10^{-8} cm^{-1}. For the thin films (<100 nm) that will likely be used for the Starshot lightsail, PDS can measure absorption down to less than 10^{-3} cm^{-1}. In contrast, conventional spectroscopic ellipsometry can only reach a sensitivity in refractive index of 10^{-3}, which translates to a sensitivity in absorption coefficient of 10^{2} cm^{-1} at a 1 μm wavelength. Ellipsometry also relies on fitting rather than direct measurement of optical constants[48,49]. For more emerging materials where sample sizes are limited to thin films and membranes, certain configurations of PDS such as the transverse configuration[50] can be used, and further effort on PDS and PAS should be dedicated to pushing the sensitivity limits below 1 cm^{-1} even for thin film samples.

Low-weight, low-index materials, such as aerogels[24–28], could be beneficial for mechanical stability and optical reflectivity of the lightsail. However, very limited data is available on accurate optical constants and properties of bulk or thin film aerogels, stressing the need for systematic research efforts in this direction. Ultimately, the absorption and optical properties for sail materials must be experimentally measured for sample thicknesses comparable to those proposed in the sail design above (<100 nm). Only then can the absorption due to interfaces, surfaces and edge defects be accounted for in the final design. These measurements can inform efforts in advanced microscopy and materials growth to identify and eliminate extrinsic defect populations in candidate materials. With such a coordinated research program, a new class of ultrahigh-quality, ultralow-absorption materials can be designed.

Design for stability

Together with careful material and structural engineering of the sail's optical and thermal properties, a rigorous analysis of the spacecraft's dynamics during acceleration is required[51]. The possibility of a laser-propelled deep-space exploration demands not only maximizing the spacecraft's acceleration and minimizing the associated heating, but also precise control over the spacecraft's trajectory. Such a demand leads to stringent requirements for passive stability during the spacecraft's acceleration. For this reason, a holistic design of the entire system (that is, laser beam, sail and payload) is of critical importance. To illustrate this paradigm, we consider a simple scenario of a laser beam–sail interaction in the ray-optics limit. In this case, the radiation force per unit area on the sail surface may be found as[52]:

$$\frac{\mathrm{d}\mathbf{F}}{\mathrm{d}S} = \frac{1}{c} I(x,y) \left[-2R(\nu,\alpha)\cos(\alpha)\mathbf{n}[\sigma(x,y)] + A(\nu,\alpha)\mathbf{z}\right] \quad (2)$$

where c is the speed of light and $\mathbf{z}$ is the direction of propagation for the incident laser beam. Here, we assume that local radiation pressure at any given (x, y) point on the sail surface (generally defined as $G(x,y,z) = \sigma(x,y) - z = 0$) is due to reflection $R(\nu,\alpha)$ and absorption $A(\nu,\alpha)$ of an optical ray with intensity distribution $I(x,y)$ incident at an angle $\alpha = \arccos(-\mathbf{n}\cdot\mathbf{z})$ on the specular sail surface with surface normal $\mathbf{n}$. For a given sail shape, $\mathbf{n}$ can be calculated explicitly as $\mathbf{n}[\sigma(x,y)] = \nabla G/|\nabla G|$. Note that due to a relativistic Doppler shift discussed earlier, the sail reflection $R(\nu,\alpha)$ and absorption $A(\nu,\alpha)$ are spacecraft velocity dependent.

Equation (2) shows that even in this simplified case the radiation pressure depends on the synergetic interplay of several key parameters: laser beam profile $I(x,y)$, sail shape $\sigma(x,y)$ and its photonic properties $R(\nu,\alpha)$ and $A(\nu,\alpha)$, implying that each of these quantities is instrumental for the overall spacecraft stability and dynamics.

For instance, a planar sail under uniform illumination ($I(x,y) = \text{const}$) and angle independent reflection ($R(\nu,\alpha) = \text{const}$) (this case is studied in Fig. 3) is unstable[53]. In particular, arbitrarily small inclination with respect to the laser beam yields off-axis force and torque (Fig. 5a). A spherical sail and, perhaps, other convex geometries may offer pathways for stabilizing spacecraft trajectory

(Fig. 5a)[54,55]. At the same time, any realistic laser illuminating over 10 m² is most likely to have a non-uniform intensity profile resulting in an additional mechanism for instability even for a stable spherical sail (Fig. 5b). Tailoring the laser beam intensity, for example, by creating regions with intensity minima that may serve to trap the sail (for example, with a doughnut-shaped laser beam) may be a possible track for creating a stable beam–sail configuration (Fig. 5b)[51,56]. Finally, together with sail shape and laser beam engineering, local (that is, angle-dependent) reflection and absorption properties of the sail may contribute further to the spacecraft stability. Specifically, careful engineering of the laser light reflection for a given sail shape and beam profile, as shown schematically in Fig. 5c (left), may add to the balancing of the spacecraft. This is where nanophotonic and metamaterial engineering concepts previously discussed may be of a particular interest[12,57].

Together with sail shape, laser beam profile and optical properties of the sail, we identify mechanical support of the sail (Fig. 5d) and mass uniformity (Fig. 5e) (which may be an issue due to imperfections of fabrication over large areas) as other key design metrics. All of these parameters have to be optimized simultaneously, which, given cutting-edge performance requirements of the entire program, implies that complex high-performance computational tools are to be developed. A conceptual illustration of a laser propelled sail is shown in Fig. 5f, where we envision a modular design with mesoscopically engineered sail parts.

Fabrication and integration challenges

While the above sections discuss theory and conceptual design along with material parameters and measurements for the lightsail, this section discusses its practical realization in more detail. In particular, we discuss techniques for synthesis, fabrication, assembly and handling of such ultrathin membrane-like, macroscopic lightsail material. Because of the extreme constraints on the mass budget, all materials required will be in thin film form. Deposition of high-quality thin films of several candidate materials such as Si, MoS_2 and dielectric aerogels is desired. While extremely high-quality glass sheets over areas of several m² can be produced using the fusion draw process, the minimum thickness of these fusion drawn glass sheets ranges from 10–50 μm[58]. With more research and development these thicknesses can be further reduced to sub-micrometre and few-nanometre levels where it becomes attractive as a low-index spacer, cladding and for support. Thin films of aerogels will be of particular interest for spacer layers between the high-index materials and to also provide structural stability. Furthermore, while silica and alumina aerogels have been produced in bulk slabs[25–27], fabrication of freestanding aerogel films is comparatively challenging[24,28] and presents opportunity for more research and investigation. There are several approaches to producing high-index semiconductor layers. For materials such as Si[59] and diamond[60], CVD methods are well known to produce very high-quality thin films with thicknesses <100 nm over large areas. With advances in silicon on insulator technology, it is possible, in principle, to produce freestanding single crystal Si films/membranes thinner than 100 nm (ref. [61]). For layered materials with van der Waals interplanar bonding such as transition metal dichalcogenides of Mo and W, powder precursor CVD and MOCVD are known techniques for synthesizing high-quality few-nm thickness films over large areas[62,63]. The advantage with layered van der Waals materials is that they can stay free of surface, interface and dangling bond defects even down to a single atomic layer. This gives them a potential advantage over three-dimensionally bonded materials such as Si or diamond, but their relative infancy in terms of research and development means it will take several more years before the material quality is optimized up to the levels of modern day Si wafers.

A critical issue aside from growth and fabrication of the sail membranes is its integration into the final sail structure. While 18-inch diameter Si wafers can be mass produced, producing uniform high-quality material over the sail size of 10 m² is still a daunting challenge. Therefore, any practical design would involve fabrication of smaller scale tiles that can be stitched or assembled together to form the final sail design. Owing to the ultrathin nature of the sail, there are limited options available for joining and welding at the atomic level. Laser and electron beam welding are well known examples for joining thin metal foils[64,65] but the ceramic nature of all above proposed materials would render all energetic beam-welding techniques ineffective for this purpose or may lead to building of stress and defects that would result in absorption. One approach in joining single crystalline sheets would be to analogously use the wafer-bonding techniques widely employed in the semiconductor industry — except in this case the bonding would occur at the edge rather than the face of the sheet. Another approach would involve construction/fabrication of an aerogel grid or mesh with holes/gaps matching the size and shape of the individual sail tiles that can fit inside them. That would allow for a non-destructive way of assembling ultrathin membranes into a larger structure without introducing defects, stress and absorption centres at the lateral interfaces. Use of ultrastrong, nanoscopic bundles of carbon nanotubes[66] or boron nitride nanotubes[67] to tether the tiles together into desired sail shape is another possible but ambitious alternative. Overall there must be a concerted research effort to develop techniques to join and integrate ultrathin, single-crystalline materials.

Conclusions and outlook

While many open questions remain for a project as ambitious as the Breakthrough Starshot initiative, our purpose here is to define basic enabling principles for laser-driven lightsail spacecraft, in an effort to stimulate further discussion and research. Full validation of the ideas raised here will await more comprehensive analysis and experimental validation that all the relevant materials criteria are achievable for a given material, photonic design and sail shape. However, a first analysis is encouraging in that known materials, coupled with new measurement and fabrication methods, may allow design of prototype lightsails suitable for interstellar laser propelled spacecraft.

Received: 14 August 2017; Accepted: 29 March 2018;
Published online: 07 May 2018

References

1. Breakthrough Starshot. *Breakthrough Initiatives* https://breakthroughinitiatives.org/Initiative/3 (2018).
2. Lubin, P. *J. Br. Interplanet. Soc.* **69**, 40–72 (2016).
3. Marx, G. *Nature* **211**, 22–23 (1966).
4. McInnes, C. R. *Solar Sailing: Technology, Dynamics and Mission Applications* (Springer, London, 2013).
5. Small solar power sail demonstrator for "IKAROS". *Jaxa* http://global.jaxa.jp/projects/sat/ikaros/index.html (2015).
6. Tsuda, Y. et al. *Acta Astronaut.* **69**, 833–840 (2011).
7. Hughes, G. B. et al. *Proc. SPIE* **9226**, 922603 (2014).
8. Fan, T. Y. *IEEE J. Sel. Top. Quantum Electron.* **11**, 567–577 (2005).
9. Liu, Z., Zhou, P., Xu, X., Wang, X. & Ma, Y. *Sci. China Technol. Sci.* **56**, 1597–1606 (2013).
10. Brignon, A. *Coherent Laser Beam Combining.* (Wiley, New York, NY, 2013).
11. Joannopoulos, J. D., Johnson, S. G., Winn, J. N. & Meade, R. D. *Photonic Crystals: Molding the Flow of Light*. 2nd edn, (Princeton Univ. Press, Princeton, NJ, 2008).
12. Yu, N. & Capasso, F. *Nat. Mater.* **13**, 139–150 (2014).
13. Palik, E. D. *Handbook of Optical Constants of Solids.* (Academic, San Diego, CA, 1998).
14. Beal, A. R. & Hughes, H. P. *J. Phys. C Solid State Phys.* **12**, 881–890 (1979).
15. Elkorashy, A. M. *Phys. Status Solidi* **149**, 747–758 (1988).
16. Aspnes, D. E., Kelso, S. M., Logan, R. A. & Bhat, R. *J. Appl. Phys.* **60**, 754–767 (1986).
17. Kannewurf, C. R. & Cashman, R. J. *J. Phys. Chem. Solids* **22**, 293–298 (1961).
18. Jackson, W. B. & Amer, N. M. *Phys. Rev. B* **25**, 5559–5562 (1982).
19. Roxlo, C. B., Chianelli, R. R., Deckman, H. W., Ruppert, A. F. & Wong, P. P. *J. Vac. Sci. Technol.* **5**, 555–557 (1987).

20. Amato, G., Benedetto, G., Boarino, L., Maringelli, M. & Spagnolo, R. *IEE Proc. A Sci. Meas. Technol.* **139**, 161–168 (1992).
21. Nesládek, M., Vaněček, M., Rosa, J., Quaeyhaegens, C. & Stals, L. M. *Diam. Relat. Mater.* **4**, 697–701 (1995).
22. Keevers, M. J. & Green, M. A. *Appl. Phys. Lett.* **66**, 174–176 (1995).
23. Webber, D. et al. *Appl. Phys. Lett.* **105**, 182109 (2014).
24. Jo, M.-H. et al. *Thin Solid Films* **308–309**, 490–494 (1997).
25. Leventis, N., Sotiriou-Leventis, C., Zhang, G. & Rawashdeh, A.-M. M. *Nano Lett.* **2**, 957–960 (2002).
26. Pierre, A. C. & Pajonk, G. M. *Chem. Rev.* **102**, 4243–4266 (2002).
27. Zu, G. et al. *Chem. Mater.* **25**, 4757–4764 (2013).
28. Wu, S. et al. *Thin Solid Films* **628**, 81–87 (2017).
29. Macchi, A., Veghini, S. & Pegoraro, F. *Phys. Rev. Lett.* **103**, (2009).
30. Johnson, S. G. *Read the Docs* http://ab-initio.mit.edu/nlopt (2008).
31. Bendsøe, M. P. & Sigmund, O. *Topology Optimization: Theory, Methods and Applications* (Springer, Berlin, 2003) .
32. Borel, P. I. et al. *Opt. Express* **12**, 1996–2001 (2004).
33. Piggott, A. Y. et al. *Nat. Photon.* **9**, 374–377 (2015).
34. Alcaraz, J. et al. *Phys. Lett. B* **490**, 27–35 (2000).
35. Alcaraz, J. et al. *Phys. Lett. B* **494**, 193–202 (2000).
36. Hoang, T., Lazarian, A., Burkhart, B. & Loeb, A. *Astrophys. J.* **837**, 5 (2017).
37. Zook, H. A. in *Accretion Extraterr. Matter Throughout Earth's History* (eds Peucker-Ehrenbrink, B. & Schmitz, B.) 75–92 (Springer, New York, NY, 2001).
38. Green, M. A. *Sol. Energy Mater. Sol. Cells* **92**, 1305–1310 (2008).
39. Timans, P. J. *J. Appl. Phys.* **74**, 6353–6364 (1993).
40. Rogne, H., Timans, P. J. & Ahmed, H. *Appl. Phys. Lett.* **69**, 2190–2192 (1996).
41. Boccara, A. C., Jackson, W., Amer, N. M. & Fournier, D. *Opt. Lett.* **5**, 377–379 (1980).
42. Jackson, W. B., Amer, N. M., Boccara, A. C. & Fournier, D. *Appl. Opt.* **20**, 1333–1344 (1981).
43. Rosencwaig, A. & Gersho, A. *J. Appl. Phys.* **47**, 64–69 (1976).
44. Vahala, K. J. *Nature* **424**, 839–846 (2003).
45. Akahane, Y., Asano, T., Song, B.-S. & Noda, S. *Nature* **425**, 944–947 (2003).
46. Zammit, U. et al. *J. Appl. Phys.* **69**, 2577–2580 (1991).
47. Holovský, J., Remeš, Z., De Wolf, S. & Ballif, C. *Energy Procedia* **60**, 57–62 (2014).
48. Yu, G. et al. *Appl. Phys. Lett.* **70**, 3209–3211 (1997).
49. Shvets, V. A., Spesivtsev, E. V., Rykhlitskii, S. V. & Mikhailov, N. N. *Nanotechnol. Russ.* **4**, 201–214 (2009).
50. Mandelis, A. *J. Appl. Phys.* **54**, 3404–3409 (1983).
51. Manchester, Z. & Loeb, A. *Astrophys. J.* **837**, L20 (2017).
52. Rios-Reyes, L. *Solar Sails: Modeling, Estimation, and Trajectory Control.* PhD Thesis, Univ. Michigan (2006).
53. Popova, H., Efendiev, M. & Gabitov, I. Preprint at https://arxiv.org/abs/1610.08043 (2016).
54. Schamiloglu, E. et al. *AIP Conf. Proc.* **552**, 559–564 (2001).
55. Benford, J. et al. *AIP Conf. Proc.* **608**, 457–461 (2002).
56. Srinivasan, P. et al. *Proc. SPIE* **9981**, 998105 (2016).
57. Xia, F., Wang, H., Xiao, D., Dubey, M. & Ramasubramaniam, A. *Nat. Photon.* **8**, 899–907 (2014).
58. Ultra-thin glass. *SCHOTT* https://go.nature.com/2uQZihl (2018)
59. Brendel, R. *Jpn J. Appl. Phys.* **40**, 4431–4439 (2001).
60. Schwander, M. & Partes, K. *Diam. Relat. Mater.* **20**, 1287–1301 (2011).
61. Maleville, C. & Mazuré, C. *Solid. State. Electron.* **48**, 1055–1063 (2004).
62. Shi, Y., Li, H. & Li, L.-J. *Chem. Soc. Rev.* **44**, 2744–2756 (2015).
63. Li, H., Li, Y., Aljarb, A., Shi, Y. & Li, L.-J. *Chem. Rev.* https://doi.org/10.1021/acs.chemrev.7b00212 (2017).
64. Petrich, M., Stambke, M. & Bergmann, J. P. *Phys. Procedia* **56**, 768–775 (2014).
65. Ogawa, H., Yang, M., Matsumoto, Y. & Guo, W. *J. Solid Mech. Mater. Eng.* **3**, 647–655 (2009).
66. Zhang, M. *Science* **306**, 1358–1361 (2004).
67. Wang, J., Lee, C. H. & Yap, Y. K. *Nanoscale* **2**, 2028–2034 (2010).

Additional information

Reprints and permissions information is available at www.nature.com/reprints.

Correspondence should be addressed to H.A.A.